CHEMICAL ENGINEERING TRANSACTIONS
VOL. 88, 2021
A publication of AIDIC
The Italian Association of Chemical Engineering
Online at www.cetjournal.it
Guest Editors: Petar S. Varbanov, Yee Van Fan, Jiří J. Klemeš

ISBN 978-88-95608-86-0; **ISSN** 2283-9216
DOI: 10.3303/CET2188089

Finding Optimized Process Conditions to Minimize Precipitations in an SO_2 Absorption Process Using Thermodynamic Process Simulation

Barbara D. Weiß[a]*, Wolfgang Fuchs[b], Michael Harasek[a]

[a] Thermal Process Engineering - Computational Fluid Dynamics, Institute of Chemical, Environmental & Bioscience Engineering, TU Wien, Getreidemarkt 9, 1060 Vienna, Austria
[b] Sappi Austria Produktions-GmbH & Co. KG, Sappi Europe, Brucker Strasse 21, 8101 Gratkorn, Austria
barbara.weiss@tuwien.ac.at

A process model to describe SO_2 absorption from exhaust gas using an absorptive magnesium-based slurry was developed in Aspen Plus® V10. The model includes the thermodynamic description of the electrolyte system $MgO\text{-}CaO\text{-}SO_2\text{-}H_2O\text{-}O_2\text{-}CO_2$, including precipitation reactions in the system. The property method electrolyte-NRTL with an asymmetric reference state was chosen as the thermodynamic method. The model was evaluated using plant data for pH value, HSO_3^- and SO_3^{--} content of the liquid phase from an industrial SO_2 absorption venturi system of the pulp and paper industry. The model shows good accuracy in describing the pH value and the combined HSO_3^- and SO_3^{--} content. Sensitivity analyses were performed to identify key parameters that influence unwanted precipitation reactions in the system and to support the optimization of the SO_2 absorption process. Temperature and the $Mg(OH)_2/SO_2$ ratio in the system were identified as key parameters influencing the formation and precipitation of sulfites. The pH value was identified as a key parameter affecting the precipitation of magnesium hydroxide. The model predicts the precipitation of $Mg(OH)_2$ at a pH value of higher than 8 and the precipitation of $MgSO_3$ trihydrate at a temperature higher than 78 °C or a slurry/SO_2 ratio higher than around 4. The performed analyses can support optimized process design decisions for SO_2 absorption processes to avoid limiting precipitation issues.

1. Introduction

The chemisorption of SO_2 is a well-established technology to reduce SO_2 emissions from SO_2 containing exhaust gas from different industries such as coal-firing plants, sintering plants, or pulp production. Besides the traditionally used absorptive slurry based on limestone (Ozyuguran and Ersoy-Mericboyu 2010), a magnesium based slurry is widely used as an absorbent with the advantage of better recyclability and higher SO_2 removal efficiencies (Liu et al. 2020). Magnesium hydroxide as an absorptive slurry gained increased attention due to the possibility of removing the pollutants SO_2 and NO_x simultaneously (Zou et al. 2019). In the pulp production industry, magnesium hydroxide is used as slurry to control SO_2 emissions and simultaneously recover the cooking liquor. Eqs(1) – (3) summarize the main reactions of the chemical recovery for magnesium-based systems:

$$MgO + H_2O \rightarrow Mg(OH)_2 \quad (1)$$

$$Mg(OH)_2 + SO_2 \rightarrow MgSO_3 + H_2O \quad (2)$$

$$MgSO_3 + SO_2 + H_2O \rightarrow Mg(HSO_3)_2 \quad (3)$$

After the combustion of black liquor, magnesium oxide is recovered from the ash and hydrated to serve as absorbent for the SO_2 removal in the absorption venturi system. There, SO_2 reacts with the slurry to form magnesium bisulfite, which serves again as cooking liquor for pulp production.

Paper Received: 12 June 2021; Revised: 27 July 2021; Accepted: 6 October 2021
Please cite this article as: Weiß B.D., Fuchs W., Harasek M., 2021, Finding Optimized Process Conditions to Minimize Precipitations in an SO_2 Absorption Process Using Thermodynamic Process Simulation, Chemical Engineering Transactions, 88, 535-540 DOI:10.3303/CET2188089

The goal of such chemical recovery system is the full reuse of required chemicals to target a closed-loop process control. However, unwanted precipitation reactions in the system can challenge this goal. Uncontrolled precipitation can lead to blockage of pipes, shortens maintenance intervals, and increases the chemical demand. Therefore, it is essential to understand the reaction system leading to precipitations when designing wet flue gas desulfurization systems. While most studies focus on removal efficiency, the issue of precipitation is often overlooked, leading to a lack of studies targeting that issue in literature. In a previous work, potential salts and their solubility data from literature were studied (Weiß and Harasek 2021). In literature, a solid database for the solubility of potential salts in water is available. However, potential precipitations are dependent on the complex present electrolyte system. A rigorous thermodynamic model can provide a tool to analyze the effect of different parameters on the precipitation by including all necessary electrolyte reactions. The MgO-H_2O-SO_2 system was previously modeled by Zidar et al. using the Rudzinsky+Pitzer-Ion activity coefficient model (Zidar et al. 1997). Steindl et al. described the same system using the electrolyte NRTL method (Steindl et al. 2008). The newer study of Si et al. applies the electrolyte NRTL method on an SO_2 absorption system based on calcium (Si et al. 2019). This study investigates the effect of temperature, pH value, SO_2, and $Mg(OH)_2$ in the system on precipitation calculated by the electrolyte NRTL method. The flowsheet and input data are based on an industrial absorption plant of the chemical recovery in the pulp industry.

2. Methods

The system was modeled as a steady-state process in thermodynamic equilibrium. The thermodynamic framework, the reaction system, and the flowsheet calculations were set and performed using the sequential modular simulation tool Aspen Plus® V10. The following summarizes the applied methodology.

2.1 Thermodynamic framework

The system was rigorously modeled using the built-in elecNRTL property method in Aspen Plus® V10. This method uses the electrolyte NRTL activity coefficient model as proposed by Chen and Evans and extended by Mock et al. The vapor phase properties were calculated using the Redlich-Kwong equation of state. As for every activity coefficient model, the activity coefficient expresses the deviation of a solution from ideality. The reference state of the system defines which state is referred to as ideal. For ions, the reference state of infinite dilution in the actual mixed solvent present was chosen (asymmetric reference state). For all other components, the reference state is that of a pure compound. The reference state for supercritical, dissolved gases, defined as Henry components in Aspen Plus®, is at infinite dilution (asymmetric reference state) at system temperature and pressure. In the studied system, SO_2, O_2, and CO_2 were defined as Henry components. All pure component and binary interaction parameters were retrieved from the standard implemented data banks in Aspen Plus® V10.

2.2 Chemical system

Aspen Plus® V10 allows the description of electrolyte systems using the true component approach. The true component approach, unlike the apparent component approach, means that all true components of the electrolyte system, including ions, salts, and molecular species, are reported. The chemical equilibrium is calculated using built-in or user-supplied parameters to describe the equilibrium constants K_{eq} as a function of temperature. If no equilibrium constants are given, the equilibrium is calculated from the reference state Gibbs free energies of the participating components. Table 1 summarizes all considered reactions and how the chemical equilibrium was calculated.

Table 1: Considered electrolyte system

Reaction	Type	Calculation of chemical equilibrium
$2\ H_2O \leftrightarrow OH^- + H_3O^+$	Equilibrium	built-in coefficients for K_{eq}
$2\ H_2O + SO_2 \leftrightarrow H_3O^+ + HSO_3^-$	Equilibrium	built-in coefficients for K_{eq}
$H_2O + HSO_3^- \leftrightarrow H_3O^+ + SO_3^{--}$	Equilibrium	built-in coefficients for K_{eq}
$H_2O + HCl \leftrightarrow Cl^- + H_3O^+$	Equilibrium	Gibbs free energy calculation
$H_2SO_4 + H_2O \leftrightarrow H_3O^+ + HSO_4^-$	Equilibrium	Gibbs free energy calculation
$H_2O + HSO_4^- \leftrightarrow H_3O^+ + SO_4^{--}$	Equilibrium	Gibbs free energy calculation
$MgOH^+ \leftrightarrow OH^- + Mg^{++}$	Equilibrium	Gibbs free energy calculation
$CaOH^+ \leftrightarrow OH^- + Ca^{++}$	Equilibrium	Gibbs free energy calculation
$2\ H_2O + CO_2 \leftrightarrow H_3O^+ + HCO_3^-$	Equilibrium	built-in coefficients for K_{eq}
$H_2O + HCO_3^- \leftrightarrow H_3O^+ + CO_3^{--}$	Equilibrium	built-in coefficients for K_{eq}
$Mg(OH)_2 \rightarrow OH^- + MgOH^+$	Dissociation	-
$Ca(OH)_2 \rightarrow OH^- + CaOH^+$	Dissociation	-

Table 1: Considered electrolyte system, continued

Reaction	Type	Calculation of chemical equilibrium
$2\ H_2O + CO_2 \leftrightarrow H_3O^+ + HCO_3^-$	Equilibrium	built-in coefficients for K_{eq}
$H_2O + HCO_3^- \leftrightarrow H_3O^+ + CO_3^{--}$	Equilibrium	built-in coefficients for K_{eq}
$Mg(OH)_2 \rightarrow OH^- + MgOH^+$	Dissociation	-
$Ca(OH)_2 \rightarrow OH^- + CaOH^+$	Dissociation	-
$MgSO_4 \rightarrow Mg^{++} + SO_4^{--}$	Dissociation	-
$MgSO_3 \rightarrow Mg^{++} + SO_3^{--}$	Dissociation	-
$CaSO_4 \rightarrow Ca^{++} + SO_4^{--}$	Dissociation	-
$CaSO_3 \rightarrow Ca^{++} + SO_3^{--}$	Dissociation	-
$MgCO_3 \rightarrow Mg^{++} + CO_3^{--}$	Dissociation	-
$CaCO_3 \rightarrow Ca^{++} + CO_3^{--}$	Dissociation	-
$Mg(OH)_2\ (s) \leftrightarrow OH^- + MgOH^+$	Salt precipitation	Gibbs free energy calculation
$Ca(OH)_2\ (s) \leftrightarrow OH^- + CaOH^+$	Salt precipitation	Gibbs free energy calculation
$MgSO_3 * 6\ H_2O \leftrightarrow Mg^{++} + SO_3^{--} + 6\ H_2O$	Salt precipitation	built-in coefficients for K_{eq}
$MgSO_3 * 3\ H_2O \leftrightarrow Mg^{++} + SO_3^{--} + 3\ H_2O$	Salt precipitation	built-in coefficients for K_{eq}
$CaSO_3 * ½\ H_2O \leftrightarrow Ca^{++} + SO_3^{--} + ½\ H_2O$	Salt precipitation	Gibbs free energy calculation
$MgSO_4 * H_2O \leftrightarrow Mg^{++} + SO_4^{--} + 1\ H_2O$	Salt precipitation	built-in coefficients for K_{eq}
$MgSO_4 * 7\ H_2O \leftrightarrow Mg^{++} + SO_4^{--} + 7\ H_2O$	Salt precipitation	built-in coefficients for K_{eq}
$CaSO_4 * 2\ H_2O \leftrightarrow Ca^{++} + SO_4^{--} + 2\ H_2O$	Salt precipitation	built-in coefficients for K_{eq}
$CaSO_4 \leftrightarrow Ca^{++} + SO_4^{--}$	Salt precipitation	Gibbs free energy calculation

2.3 Flowsheet and input data

The developed flowsheet was based on an industrial absorption unit (Figure 1).

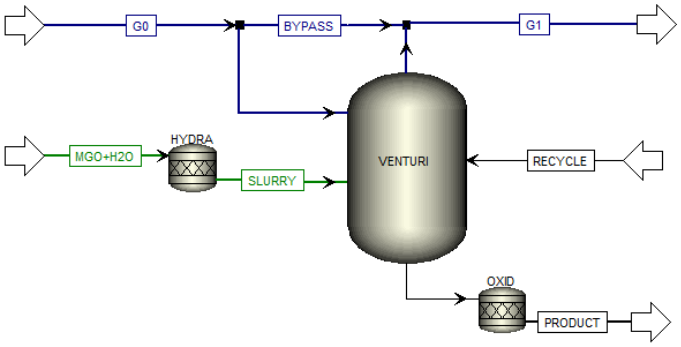

Figure 1: Flowsheet of SO_2 absorption venturi system in Aspen Plus® V10

It consists of a flash unit “VENTURI”, which calculates the chemical and phase equilibrium at atmospheric pressure of 1.013 bar and without any heat duty. In an industrial venturi system, the physical solubility of SO_2 is considered as the limiting process preventing the system to be in equilibrium (Marocco 2010). To adapt the equilibrium model to the real process, a gas bypass allows adjusting the venturi efficiency. The reactor “HYDRA” covers the hydration of MgO and CaO to $Mg(OH)_2$ and $Ca(OH)_2$ respectively, resulting in the input stream “SLURRY”. The hydration reactor was implemented as a stoichiometric reactor with a hydration rate of 90 %. The stoichiometric reactor “OXID” covers the oxidation of SO_3^{--} to SO_4^{--} in the liquid outlet of the venturi. Several studies describe the kinetics of the oxidation of SO_2 in the liquid phase. Due to the complex nature and fast kinetics of the reaction (Hudson et al. 1979), it was assumed that the total O_2 in the liquid phase reacts with SO_3^{--}. The initial composition of the exhaust gas “G0” is summarized in Table 2.

Table 2: Gas composition G0 in vol% (standard conditions, dry)

N_2	SO_2	O_2	CO_2	NO
78.43	0.41	5.94	13.52	1.71

In industrial SO_2 absorption processes, the exhaust gas usually passes several absorption units in series, and the liquid outlet of an absorption unit is recycled counter current into the previous unit. The stream “RECYCLE”

represents this liquid recycle stream. The composition of the input streams “RECYCLE” and “MGO+H2O” are summarized in Table 3.

Table 3: Composition of input streams RECYCLE and MGO+H2O in mass-%

	H_2O	$Mg(HSO_3)_2$	$MgSO_3$	$MgSO_4$	$CaSO_3$	$CaSO_4$	$MgCO_3$	MgO	CaO	N_2	Others
RECYCLE	97.20	1.66	0.82	0.04	0.07		0.03	0.08		0.06	0.05
MGO+H2O	90.95			0.34		0.04		7.84	0.35		0.48

On the presented flowsheet, sensitivity analyses were performed to study the effect of temperature, pH value and the input ratio of slurry and SO_2.

3. Results and discussion

In the following the model is validated using industrial plant data. Furthermore, results of the performed sensitivity analyses are presented and discussed.

3.1 Validation of model with plant data

Table 4 compares the calculated values of the liquid product stream with measured plant data at process conditions.

Table 4: Comparison of calculated values with data of industrial plant (with σ = standard deviation) in product (T=68 °C; $\dot{m}_{Gas0}$= 374,000 kg/h, $\dot{m}_{Recycle}$= 83,000 kg/h, $\dot{m}_{Slurry}$=3,840 kg/h, venturi efficiency = 0.55)

	Units	Calculated	Plant data
pH		5.47	5.18 σ = 0.07
SO_3^{--} + HSO_3^-	mass-% SO_2	2.94	3.04 σ = 0.22
SO_3^{--}	mass-% SO_2	0.13	0.39 σ = 0.09

The calculated amount of SO_2, which is present as SO_3^{--} and HSO_3^- in the liquid product, is in very good agreement with the measured value. The pH value shows only a small deviation of 0.22 pH units, considering the standard deviation of the measurement. Compared to measurements, the model underestimates the amount of SO_2, which is present as SO_3^{--}.

3.2 Effect of temperature on solid precipitation

Figure 2a and b show the precipitation as a function of temperature, while all other input parameters were unchanged.

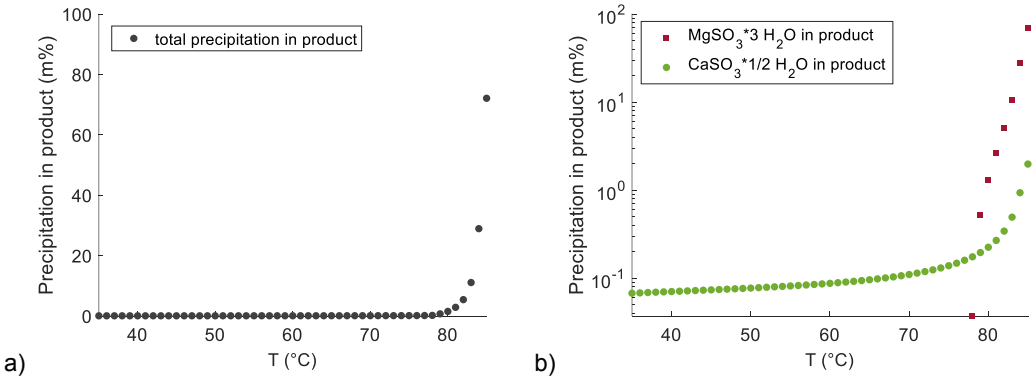

Figure 2: Precipitation in product as a function of temperature; (a) total precipitation mapped in linear scale; (b) precipitation of $MgSO_3$ 3 H_2O and $CaSO_3$* ½ H_2O mapped in logarithmic scale ($\dot{m}_{Gas0}$= 374,000 kg/h, $\dot{m}_{Recycle}$= 83,000 kg/h, $\dot{m}_{Slurry}$=3,840 kg/h, venturi efficiency = 0.55)*

The process model reports precipitation of $CaSO_3$ hemihydrate ($CaSO_3$* ½ H_2O) over the whole considered temperature range. $CaSO_3$ hemihydrate has the lowest solubility in water compared to the other considered sulfates and sulfites (Weiß and Harasek 2021). Its solubility decreases with temperature, which corresponds to the increase of $CaSO_3$* ½ H_2O in the product with temperature. However, due to the small amount of calcium

present in the system, the effect of its precipitation in the product stream is small and makes up only around 0.1 mass-% in the product. At temperatures higher than 78 °C, the model also reports $MgSO_3$ trihydrate ($MgSO_3$* 3 H_2O) as precipitated solid. This can be explained by the shift in the vapor-liquid phase equilibrium with increasing temperature. The total liquid product flow decreases with increasing temperature. As a consequence, the concentration of $MgSO_3$ in the liquid product exceeds the solubility limit leading to the precipitation of $MgSO_3$*3 H_2O. Another factor is that at higher temperatures, the less soluble $MgSO_3$*3 H_2O is the dominantly occurring form, while at lower temperatures, the more soluble $MgSO_3$*6 H_2O is the stable form (Steindl et al. 2005). The transition from hexahydrate to trihydrate as stable form can explain the precipitation of $MgSO_3$ at higher temperatures.

3.3 Effect of pH value on solid precipitation

Figure 3 shows the effect of the pH value in the system on solid precipitation.

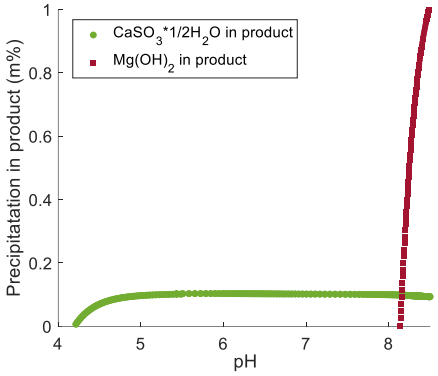

Figure 3: Precipitation in product as a function of pH value adjusted by adding HCl and NaOH (T = 68 °C, $\dot{m}_{Gas0}$= 374,000 kg/h, $\dot{m}_{Recycle}$= 83,000 kg/h, $\dot{m}_{Slurry}$=3,840 kg/h, venturi efficiency = 0.55)

The pH value was adjusted by adding HCl and NaOH to the system. HCl and NaOH were chosen as they are not part of other reactions in the electrolyte system other than their dissociation. The analyses show that $Mg(OH)_2$ precipitates when a pH value of 8 is exceeded. This corresponds to the studies by Scholz and Kahlert (Scholz and Kahlert 2015).

3.4 Effect of slurry/SO_2 ratio on solid precipitation

Figure 4a and b show the effect of the mass flow ratio of slurry and SO_2 into the venturi flash on the precipitation.

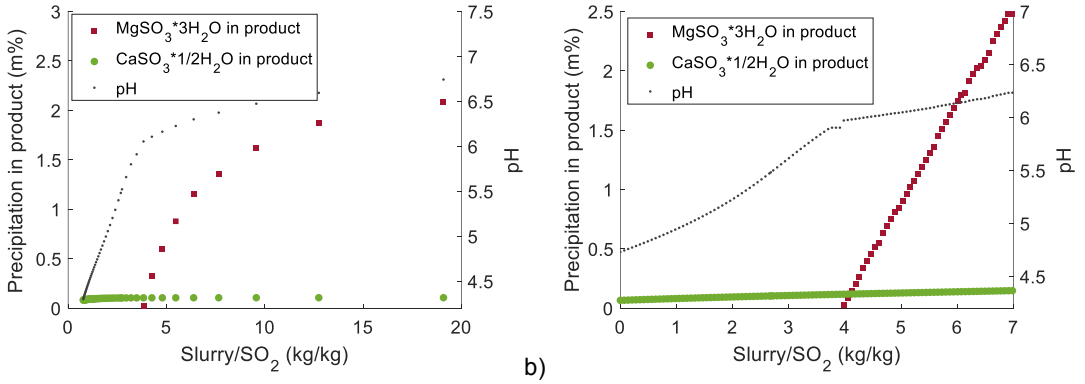

Figure 4: Precipitation in product as a function of the mass flow ratio Slurry/SO_2; (a) Varying of SO_2 input; (b) Varying of slurry input (T = 68 °C, $\dot{m}_{Gas0}$= 374,000 kg/h, $\dot{m}_{Recycle}$= 83,000 kg/h, venturi efficiency = 0.55)

The ratio was varied once by changing the SO_2 input and once by changing the slurry input. Following the Eqs(2) and (3), excess $Mg(OH)_2$ in the system leads to an increased formation of $MgSO_3$. The model reports that at a ratio higher than 4, the solubility limit is exceeded and $MgSO_3$ precipitates as trihydrate. The start of the precipitation can also be recognized by the inflection point of the slope of pH value in the product. This point is at a pH value of around 5.7 to 6.

4. Conclusions

The simulation showed promising results when compared with industrial measurement data. The performed analyses showed the importance to not only consider removal efficiency but also potential solid precipitation when designing wet flue gas desulfurization systems. The model reports $CaSO_3$ hemihydrate as precipitated solid in the product under the analyzed conditions. The precipitation of $MgSO_3$ trihydrate was reported when exceeding a temperature of 78 °C or a slurry/SO_2 ratio of higher than around 4. $Mg(OH)_2$ was reported when exceeding a pH value of 8 in the system. Those findings correspond to solubility reports found in literature. The model describes the solids occurring in the product. In a real system, local solubility exceedance can occur and lead to depositions. While the model does not depict those local concentration differences, it gives a good indication of key parameters influencing the precipitation in the system and provides a qualitative assessment of those influencing factors. Based on the performed analyses, it is recommended to ensure temperatures below 78 °C and a slurry/SO_2 ratio of lower 4 when using a magnesium hydroxide slurry. Furthermore, it is recommended to prevent exceeding a pH value of 8 to limit precipitation issues in the system. For a further evaluation of those findings, measurements using infrared spectroscopy are recommended to identify the solids and to determine the ratio of SO_3^{--} and HSO_3^- in the liquid product.

Acknowledgements

This work was financially supported by the Competence Center CHASE GmbH. CHASE Competence Center is subsidized in the frame of COMET – Competence Centers for Excellent Technologies by BMVIT, BMWFW, Wirtschaftsagentur Wien, State of Upper Austria and its scientific partners. The COMET program is handeled by FFG. The support by the project partner Sappi Papier Holding GmbH is greatly acknowledged.

References

Hudson J. L., Erwin, J., Catipovic N. M. 1979, Kinetics of Sulfur Dioxide Oxidation in Aqueous Solution, In Interagency Energy-Environment Research and Development series EPA-600/7-79-030 (EPA-600/7-79-030).

Liu X., Liao C., Le L., Gao H., Zhou J., Feng Z., Lin Z., 2020, Research progress in the environmental application of magnesium hydroxide nanomaterials. In Surfaces and Interfaces 21, p. 100701. DOI: 10.1016/j.surfin.2020.100701.

Marocco L., 2010, Modeling of the fluid dynamics and SO_2 absorption in a gas–liquid reactor. In Chemical Engineering Journal 162 (1), pp. 217–226. DOI: 10.1016/j.cej.2010.05.033.

Ozyuguran A., Ersoy-Mericboyu A., 2010, Flue Gas Desulfurization by Limestone and Hydrated Lime Slurries. In 1 19, 125–130. DOI: 10.3303/CET1019021.

Scholz F., Kahlert H., 2015, The calculation of the solubility of metal hydroxides, oxide-hydroxides, and oxides, and their visualisation in logarithmic diagrams. In ChemTexts 1 (1). DOI: 10.1007/s40828-015-0006-0.

Si T., Wang C., Yan X., Zhang Y., Ren Y., Hu J., Anthony E. J., 2019, Simultaneous removal of SO_2 and NO_x by a new combined spray-and-scattered-bubble technology based on preozonation: From lab scale to pilot scale. In Applied Energy 242, 1528–1538. DOI: 10.1016/j.apenergy.2019.03.186.

Steindl M., Röder T., Simharl R., Harasek M., Friedl A., Sixta H., 2005, Online Raman monitoring of the phase transition of magnesium sulphite hydrate. In Chemical Engineering and Processing: Process Intensification 44 (4), 471–475. DOI: 10.1016/j.cep.2004.06.011.

Steindl M., Wolfinger M. G., Friedl A., Weber H. K., Sixta H., 2008, Modelling of the Lenzing SO_2 recovery process and validation with plant data. In Journal of Cleaner Production 16 (2), 208–214. DOI: 10.1016/j.jclepro.2006.08.027.

Weiß B. D., Harasek M., 2021, Solubility Data of Potential Salts in the MgO-CaO-SO_2-H_2O-O_2 System for Process Modeling. In Processes 9 (1), p. 50. DOI: 10.3390/pr9010050.

Zidar M., Golob J., Veber M., Vlachy V., 1997, Absorption of SO_2 into Aqueous Solutions. 2. Gas−Liquid Equilibrium of the MgO−SO2−H2O System and Graphical Presentation of Operation Lines in an Equilibrium Diagram. In Industrial & Engineering Chemistry Research 36 (10), 4342–4346.

Zou Y., Liu X., Zhu T., Tian M., Cai M., Zhao Z., Wu H., 2019, Simultaneous Removal of NO_x and SO_2 by MgO Combined with O_3 Oxidation: The Influencing Factors and O_3 Consumption Distributions. In ACS Omega 4 (25), 21091–21099. DOI: 10.1021/acsomega.9b02502.